Highlights

Computational modelling of epithelial cell monolayers during infection with *Listeria monocytogenes*

Aparicio-Yuste, Raul, Serrano-Alcalde, Francisco, Muenkel, Marie, Garcia-Aznar, Jose Manuel, Bastounis, Effie E., Gomez-Benito, Maria Jose

- Contraction and protrusion of uninfected cells are identified as the key mechanism to fight infection through mechanosensing.
- The protrusion level of the cell depending on the quantitative stress asymmetry in the cells results in better predictions of mound formation in infected monolayer than an on-off protrusion law.

Computational modelling of epithelial cell monolayers during infection with *Listeria monocytogenes*

Aparicio-Yuste, Raul[a,b], Serrano-Alcalde, Francisco[a,c], Muenkel, Marie[b], Garcia-Aznar, Jose Manuel[a,*], Bastounis, Effie E.[b,**], Gomez-Benito, Maria Jose[a,**]

[a] *Multiscale in Mechanical and Biological Engineering (M2BE), Engineering Research Institute of Aragon (I3A), Department of Mechanical Engineering, Universidad de Zaragoza, Campus Rio Ebro, C/Maria de Luna s.n., Agustin de Betancourt Building, Zaragoza, 50018, Spain*

[b] *Interfaculty Institute of Microbiology and Infection Medicine, Cluster of Excellence "Controlling Microbes to Fight Infections" (CMFI, EXC 2124), University of Tuebingen , Tuebingen, 72074, Germany*

[c] *Instituto Tecnologico de Aragon (ITAINNOVA), Calle Maria de Luna 7 Zaragoza, 50018, Spain*

Abstract

Intracellular bacterial infections alter the normal functionality of human host cells and tissues. Infection can also modify the mechanical properties of host cells, altering the mechanical equilibrium of tissues. In order to advance our understanding of host-pathogen interactions, simplified *in vitro* models are normally used. However, *in vitro* studies present certain limitations that can be alleviated by the use of computer-based models. As complementary tools these computational models, in conjunction with *in vitro* experiments, can enhance our understanding of the mechanisms of action underlying infection processes. In this work, we extend our previous computer-based model to simulate infection of epithelial cells with the intracellular bacterial pathogen *Listeria monocytogenes*. We found that forces generated by host cells play a regulatory role in the mechanobiological response to infection. After infection, *in silico* cells alter their mechanical properties in order to achieve a new mechanical equilibrium. The model pointed the key role of cell-cell and cell-extracellular matrix interactions in the mechanical competition of

*Email: jmgaraz@unizar.es

**Co-last authors, both authors contributed equally to the paper.

bacterial infection. The obtained results provide a more detailed description of cell and tissue responses to infection, and could help inform future studies focused on controlling bacterial dissemination and the outcome of infection processes.

Keywords: Bacterial infection, mechanistic model, cellular and bacterial mechanobiology, finite element, *Listeria monocytogenes* .

1. Introduction

Listeria monocytogenes (*L.m.*) is a food-borne intracellular bacterial pathogen mainly affecting individuals with a weakened immune system such as elderly, pregnant women or newborns [1]. Its main route of transmission is through the ingestion of contaminated food, and its primary site of infection is the intestinal epithelium. *L.m.* can however breach this first physiological barrier *in vivo* and spread infection to secondary tissues, which often leads to fatalities in immunocompromised individuals, spontaneous abortion in pregnant women and neonatal death [2]. In 2017, 2480 cases of listeriosis were reported within the European Union, with a mortality rate of 13.8% [2]. In the same year, an outbreak in South Africa resulted in 216 deaths and 1060 confirmed cases [3]. To avoid these adverse outcomes, it is essential to advance our understanding of how *L.m.* interacts with host cells to facilitate its systemic spread and which mechanisms host cells adopt to restrict infection dissemination.

During infection of human cells, the homeostatic balance of host cells is often compromised and various alterations can occur at different scales [4, 5]. For instance, upon infection of a given epithelial cell in a monolayer *in vitro*, *L.m.* has the ability to spread to larger domains in several hours. To achieve intercellular spread, *L.m.* (and further intracellular bacterial pathogens like *Rickettsia parkeri*) reprograms infected host cells by secreting virulence factors that can alter the host cell-cell adhesion organization [6, 7]. This often leads to a weakening in intercellular force transduction thus making it easier for the bacterium to spread from one cell to another, since the stress it faces and which it needs to overcome to create and resolve a bacterial protrusion is lower [8, 9].

Although the biochemical signaling pathways that change during infection or that regulate the outcome of infection have been studied for decades, recent studies suggest that mechanical signals play also an important role

during host-pathogen interactions [8]. The biochemical and mechanical signals often crosstalk in yet to be identified ways. Human cells support their shape and execute important functions, such as migration, through a set of structural networks that span all over the cell and are largely composed by polymeric filaments. Those filaments, together with the action of motor proteins and adhesion complexes, allow cells to transmits forces to each other but also to their surrounding microenvironment and often enable them to sense it. Thus, in this complex network, multiple biomechanical interactions take place between the extracellular matrix (ECM) and the cell membrane, cytoskeleton, nucleus and other molecular entities [10].

We and others have shown that during infection with *L.m.* human cells can change the organization of their cytoskeleton and their mechanical properties [11, 12]. Moreover, we recently showed that at late times post-infection (>16 h post-infection) a mechanical competition emerges between infected and nearby uninfected cells, where stiffer uninfected surrounding cells squeeze and drive the extrusion of softer bacterially-infected cells [6, 13]. This battle between infected and surrounding uninfected cells is to a large extent mechanical in nature, and is driven by changes in the interaction between competing cell populations. However, the exact spatio-temporal changes in host cell force generation and in biochemical signaling that occur during infection and eventually lead to infected cell extrusion (*i.e.*, formation of mounds of infected cells) are not fully understood yet.

In recent years, infection processes have been a main focus of research due to the Covid-19 viral outbreak [14] but also because of the emergence of multi-antibiotic resistant bacterial pathogens [15]. Despite the relevance of developing computational tools to understand infection processes, few *in silico* models have been formulated to unravel the biomechanical interactions between human host cells, pathogens and/or their microenvironment. Most infection computational models have focused on the dynamics of bacterial propagation in colonies considering contact forces, bacterial growth or the interaction between bacteria and biomaterials, among others. However, most of the models assume bacteria as particles [16] or two-dimensional (2D) deformable bodies [5], thus ignoring its inherent three dimensional characteristics.

In this context, for example, Jasevičius et al. presented an adhesive interaction model where bacterial cells are simulated as discrete entities to analyze the interaction of bacteria with flat surfaces within a liquid medium [17]. Winkle et al. emphasized the importance of computational tools to ana-

lyze the spatiotemporal dynamics of bacterial populations. Accordingly, they proposed an agent-based model taking into account the growth of the bacteria and the mechanical interactions between bacteria, and between bacteria and their environment [18]. Bacteria *N. gonorrhoeae* was studied by Bisht and Marathe, who analyzed numerically the bacterial motility, with *tug-of-war* models, on different surfaces or channels [16]. Ivančić et al. analysed the formation of bioconvection patterns in suspensions of *Bacillus subtilis* through a set of chemotaxis–convection–diffusion equations [19]. In order to model bacterial micro-colonies interactions, Doumic et al. proposed a mechanical model studying the asymmetry of the bacteria and its friction with the substrate [20]. Additionally, Delarue et al. compared *in vitro* and *in silico* models by elucidating a collective mechanism in microbial populations, which they called self-driven jamming [21]. A further combination of both *in vitro* and *in silico* models was pursued by Grant et al. through the examination of microcolonies of *Escherichia coli*. However, in this case authors investigated the transition from 2D to 3D bacterial growth in microcolonies, they found that mechanical forces between bacteria, and between bacteria and their environment are important for the transition of the bacterial microcolony from 2D to 3D growth [5]. *L.m.* interactions with human host cells were studied by Ortega et al. through a computational model, focusing on the dynamics of intercellular bacterial spread by modeling bacteria as particles within 2D rigid (*i.e.*, non-deformable) host cells [22].

Only a few number of studies used a continuum approach by means of the Finite Element Method (FEM), to simulate bacterial interaction with biological tissues. For example, Limbert et al. presented a FEM for studying *Staphylococcus aureus* biofilm colony formation based on microscopy imaging. In this case, *S. aureus* colonies in contact with surgical sutures were simulated. The aim of this study was to predict bacterial detachment when the suture is deformed [23]. A combination of FEMs was used by Feng et al. to compute bacterial biofilm growth [24]. Velic et al. analysed bacterial growth on nanopatterned surfaces. This FEM allowed to unravel the interaction between *Bacillus subtilis* and nanopatterned surfaces via a parametric study [25]. Kandemir et al. presented an *in silico* approach for modeling bacteria-hydrogel interplay, and together with *in vitro* experiments investigated the mechanical alterations of the bacterial-hydrogel construct under different conditions [26]. Volfson et al. used Discrete Element Simulations to provide a multiscale analysis of *Escherichia coli* growth [27].

In this work, we extend our previous infection computational model [6] to

better understand how at late infection with intracellular bacterial pathogens like *L.m.* uninfected and infected cells interact, and how the latter get extruded out of the basal cell monolayer. We go a step forward, we formulate a regulatory quantitative law of the mechanobiological interactions between infected and uninfected cells. In addition, this mechanistic-law has been implemented in a FE-based approach in order to test different hypotheses about the way cell-cell and cell-ECM adhesions are distributed within the monolayer. For this aim, we have organized the paper as follows. In section 2, we describe the mechanobiological context, focusing on the main mechanical implications of infection on the biomechanics of host cells. In section 3, we present the underlying mechanobiological model of the cell monolayer during infection. Next, in section 4, we describe the numerical implementation of this model. In section 5, the main results from simulations under different conditions of infection are presented. Finally, in section 6, we discuss the results and present the main conclusions of this work.

2. Mechanobiological Context: Mechanobiology of epithelial monolayers under conditions of *L.m.* infection

L.m. can cross the intestinal epithelial barrier in an attempt to spread within the body . The intestinal epithelium consists of a single layer of cells and acts as a protective barrier that separates the intestinal lumen from the external environment (Figure 1.a left). To understand the mechanisms used by intracellular *L.m.* to spread through neighbouring epithelial cells, and to unravel the mechanical interactions between infected and neighbouring non-infected cells, *in vitro* experiments are often performed [6]. The gold standards of these experiments involve exposure of epithelial cells in monolayer to *L.m.* and examination over time of the spreading behavior of *L.m.* along these monolayers. Accordingly, it was recently shown that at late times post-infection with *L.m.*, a mechanical competition between infected and neighbouring non-infected cells takes place. In infected monolayers, the uninfected cells surrounding the infection site try to organise themselves to expel the infected cells out of the monolayer, which in turn gives rise to the formation of a mound of infected cells where infected cells pile on top of each other (Figure 1.a right). The height of the mound appears to depend on the intracellular replication of the bacteria and their spreading capacity through the monolayer, as well as on the mechanical properties of the substrate or ECM on which cells reside among other factors [28, 29]. Cell-cell

and cell-ECM adhesions play a crucial role in this process. In fact, when host cells lack key proteins involved in proper formation of intercellular adhesions, uninfected cells are unable to expel infected cells [6].

In epithelial monolayers, the mechanisms involving extrusion of single apoptotic (dying), unfit or excess cells in the context of overpopulation, have been relatively well studied [30]. Extrusion of cell(s) in the context of cancer, infections and other pathologies have also being previously examined, mostly from a biochemical perspective [31]. In fact, it is interesting to remark that depending on the cell microenvironment, the way extrusion occurs may be different. For example, single cell extrusion is observed *in vivo* in the intestinal epithelium under conditions of *L.m.* infection [22, 32]. In this context cells in the epithelial monolayer proliferate and migrate upwards, away from the intestinal crypts, leading to the extrusion of single infected cells on the tip of intestinal villi (Figure 1.a left). However, we previously observed that *in vitro* in epithelial cell monolayers infected with *L.m.*, the extrusion occurs later in infection through the formation of a mound of several infected cells, thus features of massive collective cell extrusion are apparent in this case. Despite of this collective behavior in monolayers infected with *L.m.*, other types of host cells infected with intracellular bacteria also exhibit extrusion in *in vitro* conditions. For example, single rather than collective extrusion has been shown for epithelial cells infected with the intracellular bacterial pathogen *Salmonella enterica* [33]. This disparity raises the question of what controls infected cell extrusion, what determines whether extrusion will occur in single cell or collectives and whether the underlying mechanisms are similar?

In the case of overpopulation or extrusion of apoptotic cells, the surrounding cells typically create an actin-rich ring which contracts and eventually forces the extrusion of the cell they detect as a surplus [31, 34]. However, this ring has not been observed around foci of cells infected by *L.m* [6]. The precise mechanisms used by uninfected neighbouring cells to eject *L.m.* -infected cells are not yet unambiguously delineated. Here, we extend our previous mechanobiological computational model to simulate infection of host cells in monolayer [6, 29] in order to understand the mechanisms that lead to collective infected cell extrusion.

Several experimental observations have pointed to the important mechanical alterations that occur in host cells during infection and lead to cell-cell competition followed by infected cell extrusion. Atomic force microscopy (AFM) measurements indicate that the stiffness of infected cells in mono-

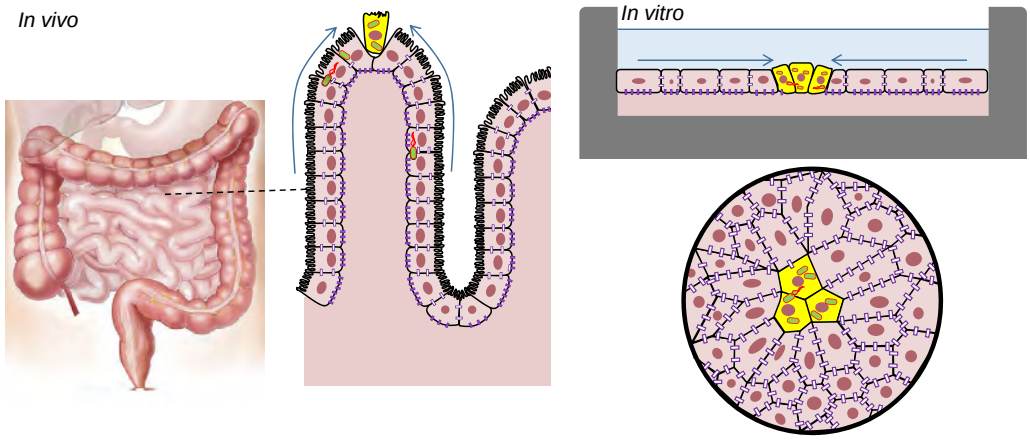

(a)

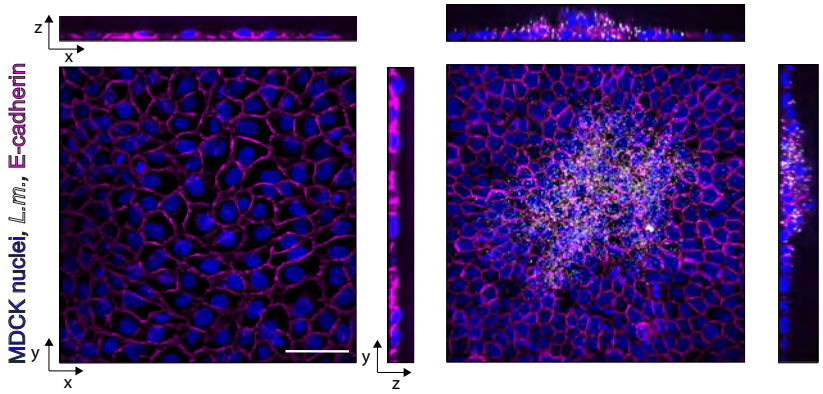

(b)

Figure 1: (a) The intestinal epithelial cell monolayer acts as a protective barrier whose organization can change during intracellular bacterial infection. *In vivo* (left) and *in vitro* (right) representation of an epithelial cell monolayer during infection. The left sketch depicts the 3D topography of the epithelial cell monolayer in the small intestine during infection with *L.m.* The right sketch shows a simplistic representation of how *L.m.*-infected cells *in vitro* are squeezed due to the forceful action of their uninfected neighbours. Nuclei (red), infected cells (yellow), *L.m.* (green), cell-cell junctions (white) and cell-ECM adhesions (purple). (Intestine image from Pixabay by Elionas2). (b) Representative orthogonal views for MDCK epithelial cells from an uninfected well (left) and for *L.m.*-infected well around an infection focus at 24 hours post infection (right). Orthogonal views show host cell nuclei in blue, *L.m.* in white and E-cadherin to mark cell-cell junctions in magenta. Scale bar is 50 μm.

layer is reduced to approximately half the stiffness of the surrounding uninfected cells [6]. As a result of this reduction in cell stiffness accompanied by alterations in the cells' cytoskeleton, infected cells exert lower traction forces on the surrounding ECM. Concurrently, the neighbouring uninfected cells adjacent to the infection domains stiffen and exert increased traction forces on their ECM. These alterations lead to a competition between infected and neighbouring uninfected cells due to a stress gradient generated along them (Figure 1.b). We believe that one of the keys to understanding this dynamical process is to determine the precise mechanical alterations that occur across host cells during infection [12], the stresses to which host cells are subject to and the interaction forces between cells and their ECM. This in turn can shed light into the mechanobiological mechanisms that intracellular bacteria employ to facilitate their spread, and conversely into the actions that host cells can take to obstruct the dissemination of the infection.

3. Mechanobiological model of a cell monolayer infected with *L.m.*

To reproduce the *in vitro* experiments, we formulate a model to mimic the interaction of infected cell domains surrounded by uninfected cells when those form a monolayer as described before [6]. The aim of our model is to simulate a particular stage of infection, arising between 8 to 16 h. post infection, when *in vitro* a mechanical competition arises between bacterially-infected versus surrounding uninfected cells. At this particular stage, uninfected surrounding cells sense the mechanical gradient at the border of the infection domain, and as a result polarise and collectively move towards the infection focus squeezing and eventually forcing the extrusion of infected cells [6]. To simulate this specific stage of infection, we take into account three important experimental measurements we previously conducted during *in vitro* infection: (a) Uninfected surrounding cells exert large traction stresses on their ECM since they grab the ECM and pull it away from the infection focus as they migrate towards it. (b) Uninfected surrounding cells are polarized and directionally migrate towards the infection focus. (c) There is a gradient in cellular traction stresses and monolayer stresses between infected and surrounding uninfected cells [29]. To simulate the cell monolayer and the mechanical interactions between infected and uninfected cells, we hypothesize a mechanotransduction mechanism based on these previous experimental observations [6]:

1. First, each single cell contracts, which allows uninfected cells to sense mechanical alterations in their microenvironment due to the presence of infected cells nearby (phase 1 in Figure 2).
2. If cell-cell junctions are properly formed, the adhesions of the cell to the ECM initially present a low stiffness, so that the cell displaces itself relative to its ECM. If the relative displacements between the cell and the ECM are large, the cell creates stiffer cell-ECM adhesions (phase 2 in Figure 2). This results in a collective cell behaviour, which is based on previous works in which authors simulate monolayers migration in response to a gradient of ECM stiffness [35, 36]. If new cell-ECM adhesions are created the cell will contract again to sense the new mechanical environment (phase 1).
3. If the cellular displacements relative to the ECM are small (with or without stiff cell-ECM adhesions), then the given cell might or might not experience a stress asymmetry depending on the mechanical state of its neighbouring cells (phase 3 in Figure 2).
4. At this point, if the given cell experiences a stress asymmetry, it creates a protrusion towards the side of minimal stress and thereby polarizes in that given direction. In this work, we consider that the mechanical states of the cell are guiding cell polarization as shown in previous works [37, 38]. We hypothesize that the level of protrusion is proportional to the level of stress asymmetry inside the cell (phase 4 in Figure 2).

In the *in vitro* experiment, there is probably a tightly regulated interplay between the polarization of a given cell and its contractile behaviour, but whether protrusion of the cell follows strong contraction, and such a cycle repeats quasi-periodically is not yet known. However, there is evidence in other cellular systems, for example, in single or streaming *Dictyostelium discoideum* cells and in immune cells, that protrusion of the leading edge is followed by contraction of the cell in a motility cycle that appears periodic [39, 40]. Therefore, our model, although not explicitly tested for MDCK cells in monolayer, is based on behaviours observed in other cellular systems.

Apart from our proposed mechanotransduction mechanism, for both infected and uninfected cells, we model the mechanical cell behavior, distinguishing between the passive and active behaviour. On the one hand, the passive part represents the capacity of the cell to be passively deformed and can be mainly attributed to the cell cytoskeleton. On the other hand, the active behaviour of the cell is defined by their capacity to generate forces

through the active action of the actomyosin contractile apparatus [41, 42]. Within the mechanotransduction mechanism, the active response of the cell to sudden changes in stress is meant to generate a protrusion in the front part of the cell and an asymmetry in the cell configuration. In our previous model, the protrusion [6] was implemented as on-off law. By using this model, if there is an asymmetry in stresses the cell always protrudes to the same degree, no matter how small or large the stress asymmetry is. Here we hypothesize that the cell protrudes proportionally to the stimulus that it is sensing. When the asymmetry of the cell is higher, the protrusion response of the cell is also higher as opposed to lower levels of stress asymmetry. Therefore, a linear protrusion law is proposed as a function of the difference in stresses (equation 1). We also assume that uninfected surrounding cells are polarized towards the infection domain, where the traction and monolayer stresses are weakened. Through *in vitro* detailed analysis we previously showed that in *L.m.*-infected cell monolayers, neighbouring uninfected cells exhibit a strong radial alignment pointing towards the centre of the infection focus, where additionally the traction and monolayer stresses are weakened [6, 29]. Thus, in our model the protrusion occurs in the front part of the cell (the part of the cell in which maximal principal stresses are lower), and this protrusion is proportional to the stress asymmetry inside the cell:

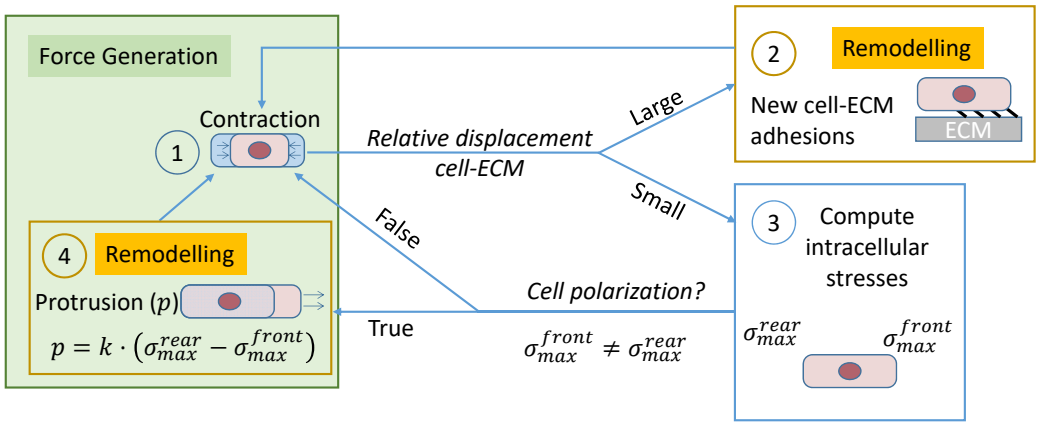

Figure 2: Cell mechanotransduction scheme. We propose two active phases (contraction (1) and protrusion (4)) and one passive phase, where the cell behaves depending on the mechanical stimulus that it is sensing. Cell protrudes (4) only under two conditions: when cellular displacements relative to the ECM are small (3) and if there is stress asymmetry in the cell.

$$p = k \cdot (\sigma_{max}^{rear} - \sigma_{max}^{front}) \tag{1}$$

where p is the level of protrusion, k is constant and σ_{max}^{front} and σ_{max}^{rear} are the averaged maximum principal stress of the front and rear part of the cell, respectively. The range of values of the parameter related to the level of protrusion (k) are chosen to obtain a sufficient level of cell protrusion so that squeezing of infected cells would emulate the corresponding experimental stage of infection just prior to infection mound formation.

To simulate either the contraction or the protrusion of the cell, we assume both of them produce volumetric changes of the cell in the plane of the monolayer. We consider three configurations, the undeformed ($\mathbf{\Omega}_0$), the deformed ($\mathbf{\Omega}_t$) and one intermediate ($\mathbf{\Omega}_i$), and these configurations can result either due to contraction or to protrusion (which in general are non-compatible) [43, 44]. The total deformation gradient which maps the point of the undeformed configuration ($\mathbf{X}$) to the points in the deformed ($\mathbf{x}$) is:

$$\mathbf{F} = \frac{\partial \mathbf{x}}{\partial \mathbf{X}} \tag{2}$$

We make use of the multiplicative decomposition [45] of the total deformation gradient $\mathbf{F}$:

$$\mathbf{F} = \mathbf{F_e} \cdot \mathbf{F_i} \tag{3}$$

where $\mathbf{F_e}$ represents the pure elastic deformation, whereas $\mathbf{F_i}$ is the growth deformation gradient produced by the volume change due to the contraction or protrusion of the cell:

$$\mathbf{F_i} = \begin{cases} \begin{pmatrix} (1+\frac{p}{2}) & 0 & 0 \\ 0 & (1+\frac{p}{2}) & 0 \\ 0 & 0 & 1 \end{pmatrix}, & \text{protrusion} \\ (1-c)\mathbf{1}, & \text{contraction} \end{cases} \tag{4}$$

where c is a constant related to the volumetric contraction of the cell which is assumed equal in all cells, $\mathbf{1}$ is the second order unit tensor.

The Cauchy-Green Tensor $\mathbf{b}$ [46] is related to the total deformation gradient by:

$$\mathbf{b} = \mathbf{F} \cdot \mathbf{F^T} \tag{5}$$

A decoupled representation of the strain energy function is adopted here since we consider both active and passive cell contributions, we assume the deformation of both are equal:

$$W(\mathbf{b}) = W_{passive}(\mathbf{b}) + W_{active}(\mathbf{b}) \tag{6}$$

where $W(\mathbf{b})$ is the strain energy function, $W_{passive}(\mathbf{b})$ and $W_{active}(\mathbf{b})$ are the corresponding passive and active strain energy functions, respectively. Therefore, the stress tensor associated to each passive and active part is defined as:

$$\sigma_{\mathbf{passive}} = 2J^{-1}\mathbf{b}\frac{\partial W_{passive}(\mathbf{b})}{\partial \mathbf{b}} \tag{7}$$

$$\sigma_{\mathbf{active}} = 2J^{-1}\mathbf{b}\frac{\partial W_{active}(\mathbf{b})}{\partial \mathbf{b}} \tag{8}$$

where J is the Jacobian determinant.

4. Mechanical model implementation

We simulate a cell monolayer in which cells in the center are infected with *L.m.* to reproduce a particular stage of infection (Figure 3.a). For the sake of simplicity, we assume the deformations and strains in the cell monolayer and its substrate are small. In fact, we focus on the short-term reaction of uninfected cells to infection, rather than on the long-term reaction or the complete extrusion of infected cells out of the monolayer. Thus, the model is implemented under the infinitesimal strain theory.

4.1. Cell model

To simulate the cell domain, we assume both parts of the cell (the active and passive one) work in parallel, assuming a linear elastic material where the total stress Cauchy tensor of the cell, under the small strain assumption, is the sum of the passive and the active contributions:

$$\boldsymbol{\sigma}_{cell} = \boldsymbol{\sigma}_{passive} + \boldsymbol{\sigma}_{active} \tag{9}$$

we assume same deformations for both passive and active parts:

$$\boldsymbol{\varepsilon}_{cell} = \boldsymbol{\varepsilon}_{passive} = \boldsymbol{\varepsilon}_{active} \tag{10}$$

where $\boldsymbol{\sigma}_{cell}$ is the total Cauchy stress tensor of the cell, $\boldsymbol{\sigma}_{passive}$ and $\boldsymbol{\sigma}_{active}$ are the Cauchy stress tensors of the passive and active part of the cell respectively; $\boldsymbol{\varepsilon}_{cell}$, $\boldsymbol{\varepsilon}_{passive}$ and $\boldsymbol{\varepsilon}_{active}$ are the Cauchy strain tensors of the cell, its passive and active part respectively.

According to the experimental AFM measurements we previously conducted [6], we consider that infected cells get softer than surrounding uninfected cells. We set the total elastic modulus (E_{cell}) to $1000\boldsymbol{Pa}$ for uninfected cells and $250\boldsymbol{Pa}$ for infected cells. As a first approach, we assume that both, passive ($E_{passive}$) and active (E_{active}) elastic moduli, are $500\boldsymbol{Pa}$ for uninfected cells and $125\boldsymbol{Pa}$ for infected cells, values that are consistently close to experimental observations [6]. A sensitivity analysis of the effect of differential cell stiffness between infected versus surrounding uninfected cells on promoting infection mounding can be found elsewhere [29].

The Poisson's ratio for the passive part is set to 0.48, thus we assume it is nearly incompressible [42]. The active part mainly represents the actomyosin-generated cell contraction and actin polymerization; we consider that contraction is not isotropic but it mainly occurs in the plane of the monolayer [47]. Thereby, the Poisson's ratio is assumed 0 to uncouple the vertical direction of the active part of the cell and the monolayer plane effects. Hence, we assume the cytoskeleton is organized to induce the maximum contraction in the plane of the monolayer.

To simulate contraction, protrusion and cell adhesion in a simple way, we divide the cell body in three differentiated zones: contractile, adhesive and protrusive zones respectively (Figure 3.b). The contraction of the cell is simulated in the cell center, where we assume that the acto-myosin apparatus is located. At the side edges of the cell we assume F-actin polymerization takes place thus regulating cell protrusion. Between the contractile and protrusive zones, we set the adhesive zone, where the cell can adhere to the ECM. Finally, we add cell-cell junctions assuming that all cellular side areas are connected to neighboring cells. This domain separation or the division of the cell body is assumed in order to consider in one geometrical continuum cell model the two main processes that generate forces: contraction and protrusion. The simulations were run with a value of the parameter k (equation 1, protrusion law) equal to $3.5{\cdot}10^{-5}$ mPa^{-1}. Higher values of the parameter k lead to larger protrusions p and convergence issues in the cell-ECM contact

surfaces since some cells might penetrate the ECM. Additionally, to determine cell polarization, each cell is divided into six triangular prisms in order to define the front and the rear part of a given cell. Afterwards, the average maximum principal stress is computed in each of these prisms. The prism subjected to the highest maximum averaged principal stress is defined as the rear part of the cell, whereas the prism opposite to this one is the front part of the cell.

4.2. Cell-cell and cell-ECM adhesions

Regarding the cell mechanical interactions, we consider both cell-cell and cell-ECM adhesions. On the one hand, cell-cell junctions are modelled by introducing in the geometry of the model a continuum element between both neighbouring cells (Figure 3.b). This element is a thin sheet modelled with a linear elastic constitutive behaviour. Following the experimental work of Bastounis et al.[6], we simulate the inhibition of cell-cell junctions by decreasing the Young's modulus of the cell-cell junctions to values close to zero (Table 1). By doing so, the force transmission between neighbouring cells is disrupted. Thus, when cell-cell junctions cannot get established because important relevant proteins are knocked out, cells do not interact anymore. On the other hand, cell-ECM adhesions are simulated as cohesive contacts. The cohesive contact used in the model follows the uncoupled traction-separation law, where the contact exhibits a linear behavior that is defined by the stiffness in three directions: normal direction to the contact surface and the two in-plane shear directions. Therefore, the elastic behavior can be written as follows:

$$\mathbf{t} = \begin{Bmatrix} t_n \\ t_s \\ t_t \end{Bmatrix} = \begin{bmatrix} K_{nn} & 0 & 0 \\ 0 & K_{ss} & 0 \\ 0 & 0 & K_{tt} \end{bmatrix} \begin{Bmatrix} \delta_n \\ \delta_s \\ \delta_t \end{Bmatrix} = \mathbf{K}\boldsymbol{\delta} \tag{11}$$

where $\mathbf{t}$ is the the stress vector, $\mathbf{K}$ is the stiffness matrix and $\boldsymbol{\delta}$ the separation of the cohesive contact. Subscripts n, s and t denote the normal and shear directions to the surface. It should be noted that the cohesive behavior is not introduced as elements, but as a cohesive contact. Therefore, the units of stiffness are $[Force/volume]$.

This type of contact allows the bonding of two different meshes and the control of stiffness in the normal and shear direction of this cell-ECM adhesion. In this case, we also consider two possible behaviors depending on whether cell-cell junctions are properly formed or not. If cell-cell junctions

are formed in our simulation (and thus cells behave as a collective), the cell-ECM adhesion forces are weaker compared to the case where cell-cell junctions cannot form. In this latter case, cells behave more as individual entities. When we assume weaker cell-ECM adhesion, the stiffness in the normal direction is $10nN/\mu m^3$ and negligible in the shear direction. On the contrary, when we consider more rigid cell-ECM traction forces, the stiffness in the normal and shear direction is $1000nN/\mu m^3$. Each cell has a total contact area of $31.61\mu m^2$ (six zones of $5.268\mu m^2$). Therefore, the total active adhesion forces (traction forces) of each cell to the ECM are $31.61nN/\mu m$ and $31608nN/\mu m$ for the lower and higher rigid adhesion, respectively. This behavior has been observed experimentally in previous works measuring the traction forces of cells exerted on their ECM when migrating on an ECM that exhibits a gradient of stiffness [36]. In this study, cells are thought to work collectively which allows them to detect different ECM stiffness and move towards the stiffer ECM side (durotaxis). This assumption has been successfully implemented in a previous computational work [35]. Finally, all the adhesion properties are summarized in Table 1. The cell-ECM adhesion parameter is estimated through a sensitivity analysis and is calibrated to obtain the sufficient level of adhesion between the ECM and the cell, but we find that up to a certain value, the alterations in cell displacements in the model are minimal.

		Base case scenario	Cell-cell contact inhibition	New cell-ECM adhesion
Cell-cell Junction	Elastic Modulus (Pa)	1000	0	1000
	Shear Modulus (Pa)	500	0	500
Cell-ECM Adhesion	Normal direction ($nN/\mu m^3$)	10	1000	1000
	Shear direction ($nN/\mu m^3$)	0	1000	1000

Table 1: Summary of cell-cell junction and cell-ECM adhesion properties. We consider the cell-cell contact inhibition when cells are not able to form cell-cell junctions and cells exhibit an increase in their cell-ECM adhesion strength. Additionally, we also consider the creation of new cell-ECM adhesions near the infection focus following the mechanotransduction mechanism. The new cell-ECM adhesion only increases the stiffness of the adhesion in neighbouring uninfected cells.

4.3. Finite element model

We simulate a cell monolayer formed by 1 600 cells on a flat planar ECM (Figure 3.a). We assume that cells are arranged in the monolayer as regular hexagons with side length and thickness of $7\mu m$ [48]. To simulate the infection, we initially consider an infection focus comprised by seven infected cells in the center of the monolayer. Thus, the boundary effects in the region of interest are neglected, since the domain is large enough to assume Saint-Venant's principle in the region of interest (infected cells and uninfected cells close to the site of infection). In addition, we apply a non-displacement boundary condition on the exterior side of the cells that are at the border of the monolayer, thus we assume that the displacements far from the infection are negligible. The ECM is also large enough to avoid border effects, we assume it as a linear elastic material (elastic modulus 3kPa and Poisson's ratio 0.3). In terms of time scale, we only analyze a short period of time in which only one mechanotransduction cycle is simulated. This cycle could be repeated several times and the displacements would be more prominent. Nevertheless, from the mechanical point of view, one cycle is sufficient to analyze the behavior of cells at this particular stage of infection when competition occurs.

The model is implemented in the commercial finite element software (FE-based) ABAQUS [49] (Figure 3.a). To simulate the passive and active behavior of the cell, we create two overlapping meshes sharing the nodes of the cells. This mesh is discretized with linear wedge elements of average size $2\mu m$ and 270 elements for each part of the cell, active and passive (540 total elements for each cell). The cell-cell junctions are modeled with nine linear hexahedral elements per contact face and the ECM is modeled with 117 600 linear hexahedral elements. The total number of elements in the model is 1 024 800 and 606 232 nodes. We performed a refinement analysis of the mesh size, and we conclude that the current mesh is suitable due to the computational cost and the results we retrieve, since the stress distribution and magnitude are closely similar to other finer meshes. We should keep in mind that our aim is to analyse the qualitative differences during infection in the various mechanical scenarios in order to find the causal relationships that modulate the outcome of the competition between bacterially-infected or uninfected cells.

Overall, we initialize our computational model taking into account the previous considerations to simulate the behavior of a cell monolayer comprised of an infection focus of seven infected cells and adhering on an ECM.

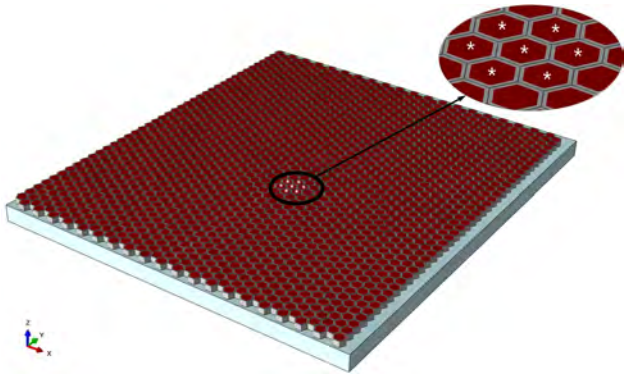

(a)

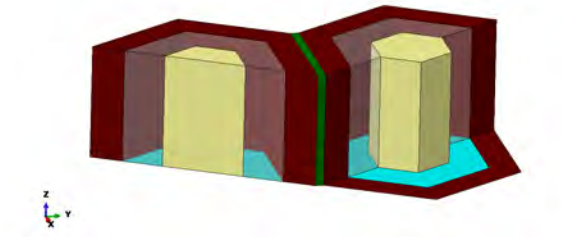

(b)

Figure 3: (a) Computational model of the cell monolayer composed by 1 600 cells and their ECM. Cells are in red oxide and gray (gray color for the protrusion zone of each cell to make easier cells' visualization) and the ECM in light blue. The zoomed region corresponds to infected cells (marked with an asterisk). (b) Scheme of the cell parts considered: contractile (yellow), protrusive (red oxide), adhesive (light blue) and cell-cell junction (green).

The computational domain is defined by the geometry of the model (the cell and ECM), whose mechanical properties are considered based on our experimental observations [6], assuming a linear elastic material behavior. The different domains are connected through specific mechanical interactions (cell-cell and cell-ECM adhesions) and implemented in two differentiated meshes for the cell domain (active or passive behaviors). Altogether, this approach allows us to run a FEM analysis and examine the displacements and principal stresses in both the ECM and the cell domain during a particular stage of infection. The computational scheme is summarized in Figure 4.

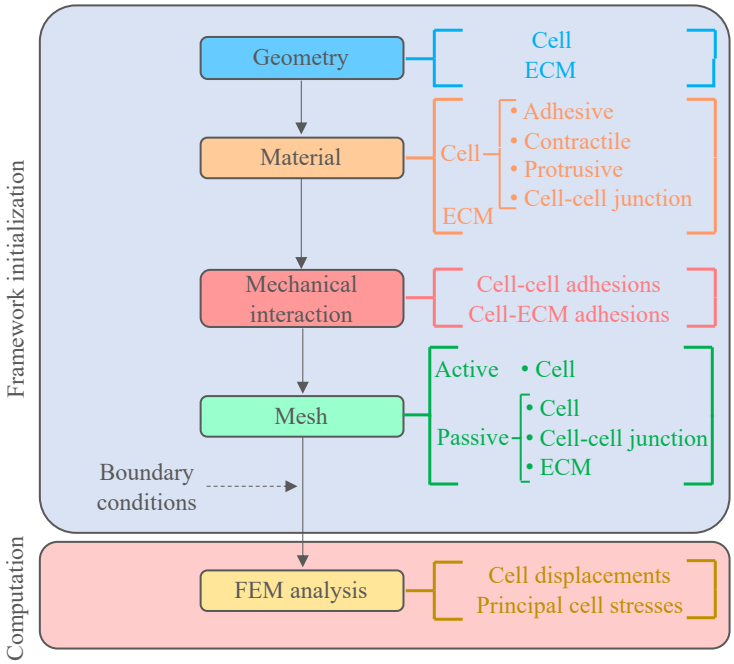

Figure 4: Computational scheme of the mechanical model

4.4. In silico simulations

Given the complexity and dynamics of bacterial infection, we aim to test quantitatively and independently at this stage: (1) whether the existence of strong cell-ECM adhesions at the border of the infection domain influences the squeezing of infected cells, since cell monolayer stresses are concentrated at the interface between infected and surrounding uninfected cells [29], (2) whether inhibition of cell-cell junctions that are distant from or near to the site of infection disrupts the intercellular force transmission, therefore attenuating the collective squeezing and subsequent extrusion of infected cells, (3) the influence of our proposed stress asymmetry-dependent protrusion law in the squeezing of infected cells and subsequent formation of the infection mound and how the *in silico* model compares to our previous model that was based on an on-off protrusion law.

We analyse four scenarios with the new proposed protrusion law. Additionally, we compare these scenarios with our previous results [6] where the new protrusion law was not considered, since protrusion was determined by an on-off law. In the first two scenarios our attention is focused on whether

cell-ECM adhesions are relevant to cell remodelling during bacterial infection, whereas in the third and fourth scenarios we analyse the role of cell-cell junctions in the collective cell behavior during infection. The size of the infection is fixed to seven cells in the center of the monolayer in all the cases, and those are the cells that present different mechanical properties (less stiff than uninfected cells). The different scenarios are enumerated as follows:

- *Case 1*: no new cell-ECM adhesions are produced around the site of the infection. Thereby, the cellular remodelling due to creation of new cell-ECM adhesions is not activated in the model when uninfected cells sense relative large cell-ECM displacements (Figure 2). The adhesion properties correspond to the base case scenario in Table 1.

- *Case 2*: the general cell-ECM adhesion properties correspond to the base case scenario (Table 1). However, when uninfected cells close to the infection site detect large displacements relative to their ECM, they create new strong cell-ECM adhesions. The new cell-ECM adhesion properties of neighbouring uninfected cells close to infection are shown in Table 1.

- *Case 3*: cell-ECM adhesions and consequently, the cell remodelling close to the infection site are considered to be the same as case 2. However, cell-cell junctions formed by cells far from the infection site are inhibited (*i.e.,* distal cell α in Figure 5.a). The new cell-cell contact inhibition properties are illustrated in Table 1.

- *Case 4*: cell-ECM adhesion properties are selected based on case 2. However, cell-cell junctions close to the infection site (*i.e.,* proximal cell β in Figure 5.a) are inhibited as opposed to the situation in case 3.

5. Results

5.1. Epithelial cells exhibit different mechanical states when infected which depend on their location

First, we address the question of whether all the cells of the monolayer that reside on a planar elastic ECM are able to sense the mechanical differences produced by the infection with *L.m.* To do so, we analyze the scenarios introduced before.

The mechanotransduction cycle we present consists of different phases. During the contraction phase, we observe stress asymmetry in all four scenarios (Figure 5.b, left). By stress asymmetry, we imply that cells are sensing a gradient of stresses. However, the degree of asymmetry is different depending on the specific scenario. We can distinguish two types of stress asymmetry: (1) a local cell stress asymmetry, considering the cell itself as an entity, or (2) a global monolayer stress asymmetry, where cluster of cells exhibit different levels of stress. The global asymmetry in stresses is more pronounced in the scenarios where new strong cell-ECM adhesions are formed around the infection focus, in response to large cell-ECM displacements (cases 2, 3 and 4 in Figure 5.b, left). For example, in those cases, the stress distribution of distal cells (α cells) contrasts significantly with respect to proximal cells (β cells).

Given the fact that new cell-ECM adhesions are formed, cases 2, 3 and 4 also exhibit different global stress distributions. In case 2, all the cell-cell junctions are simulated whereas in case 3 and 4 we inhibit the cell-cell junctions distal and proximal to the infection focus, respectively. The result is that in case 2 the stress distribution between distal (α) and proximal (β) cells is more similar than in cases 3 and 4. The inhibition of cell-cell junctions leads to a low level of stresses, meaning that cells are not able to transmit forces between each other. The cell that senses low level of stresses is the distal (α) cell in case 3 and the proximal (β) cell in case 4, corresponding to the cells that present inhibited junctions.

Altogether these findings suggest that the cell-ECM and cell-cell adhesions close to the infection focus crosstalk and guide the response of cells in the monolayer in response to infection, experiencing a major gradient of stresses.

5.2. The level of cell stress asymmetry depends on cell adhesions

We have shown that cells close to the infection focus play a critical role in guiding the infection process and ultimate outcome [6]. Therefore, we wondered how can uninfected cells surrounding the infection site sense their mechanical microenvironment and how does this mechanical input affect the stress asymmetry of the cell?

Given the protrusion law we propose, here we examine the role of the level of cell protrusion (p) in modulating the behavior of the infected cell monolayer. Particularly, we are interested in the local cell stress asymmetry that proximal (β) cells present, since those are the cells that surround

the infection focus. Once a cell contracts, following our proposed mechanotransduction cycle, the protrusion only occurs when the maximum principal stresses between the front and rear part are distinct. In this context, we observe that the modulation of the adhesions influences the level of protrusion.

The local stress asymmetry in proximal (β) cells is low for cases 1 and 4, where new cell-ECM adhesions or cell-cell junctions at the site of the infection are inhibited, respectively. For that reason, the displacements during the protrusion phase are low (Figure 5.b, right), as well as their stress asymmetry or protrusion level (Figure 6.a). For example, in case 1 the degree of asymmetry is low (lower than 0.01%) and so is the protrusion. However, when new cell-ECM adhesions are formed at the border of the infection and cell-cell junctions are not inhibited in that region (case 2 and 3), proximal β cells exhibit larger local cell stress asymmetry leading to larger displacements towards the infection, producing a longer protrusion (Figure 5.b). In case 2 all the cell-cell junctions are bearing loads whereas in case 3 only the ones close to the infection site. This fact results in a different local stress asymmetry between both cases, being 2 the case that produces a higher level of protrusion (Figure 6.a).

Additionally, in order to compare the behaviour of the computational model between the new condition (protrusion law, equation 1) and the previous work (on-off constant protrusion [6]), we compare the displacements of infected cells during the protrusion phase. The evaluated variable is the mean vertical displacement of infected cells. As explained before, the level of protrusion is proportional to the level of asymmetry. We set that the larger protrusion that cells can experience is the protrusion that case 2 exhibits. This case shows larger stress asymmetry and larger displacements in the original model, so we normalize the level of protrusion with respect to this case. Thus, the mean vertical displacements in case 2 are the same with constant protrusion or the linear protrusion law (Figure 6.b), whereas in the other three cases the result might differ. For example, in case 1 infected cells move due to a slight protrusion with the on-off model, whereas through the new protrusion law, the displacements are negligible. In the same way, the protrusion obtained in case 3 (55 % level of protrusion) is less pronounced as compared to the original model. Finally, the level of protrusion in case 4 (18 %) is not enough to present differences between both models (Figure 6.b).

When simulating case 2 and 3 with the on-off protrusion law, the model is able to yield infected cell squeezing in both cases. The model predicts the same amount of squeezing (0.8 µm, Figure 6.b) when there is no inhibition

of cell-cell junctions (case 2) or when cell-cell junctions of distal uninfected cells are inhibited (case 3). In previous experimental work [6], we observed that when two populations of cells are mixed (wild-type cells and αE-catenin knockout cells which cannot form proper cell-cell junctions), the cells that are able to form cell-cell junctions move towards the infection focus contributing to infected cell squeezing. However, the volume of the resulting infection mound is lower than that of a mound of wild-type cells. The previous on-off model predicts the same amount of infected cell squeezing in both cases (2 and 3), whereas the new linear protrusion law is able to predict less infected cell squeezing in case 3, improving the performance of the model and being more consistent with our experimental observations [6]. This difference is due to the different degree of asymmetry in mechanical stress inside the cell, being 20% and 10% in case 2 and 3, respectively. This result suggests that when all neighbouring cells are able to transduce intercellular forces and act collectively, infected cell squeezing is enhanced, whereas when some neighbouring cells cannot transduce intercellular forces, the collective cellular response that leads to infected cell squeezing is attenuated.

The findings shown here make more remarkable some of the results observed in previous works [6]. First, the relevance of the formation of new adhesions to the ECM in the cells close to the infection (case 1 vs case 2) in order to create a gradient of stresses. Second, the monolayer exhibits a lower gradient of stresses when only few uninfected cells are able to create cell-cell adhesions (case 2 vs case 3). Third, the lower ability of uninfected cells to protrude against infected cells when cell-cell junctions close to the infection are inhibited (case 3 vs case 4).

5.3. The collective cell response reproduces mound formation in a particular stage of infection

All the previous results point to the importance of cell-cell and cell-ECM adhesions in guiding (or not) the protrusive behavior of uninfected cells towards infected ones in monolayers. To test how these protrusions affect the behavior and kinematics of the cell monolayer, we examined the displacements after one cycle of contraction-protrusion.

We found that the larger displacements are exhibited in cases 2 and 3, where the level of protrusion is high enough to produce the squeezing of infected cells. The degree of asymmetry, and consequently, the degree of protrusion in cases 1 and 4, is remarkably low, thereby no large displacements are shown by infected cells (Figure 7). On the contrary, case 2 and

case 3 exhibit large displacements due to the efficient force generation from uninfected surrounding cells. As we mentioned before, case 2 exhibits even larger displacements than case 3 due to the fact that all cell-cell junctions are active in the whole cell monolayer.

We can conclude that when the force generation machinery works correctly, the cell monolayer presents a collective behavior whereby uninfected cells surrounding the infection are polarized towards the center of the infection, squeezing infected cells and allowing the formation of the mound.

6. Discussion and conclusions

In this work, we have expanded and mathematically formulated our previous computational model that simulates the mechanical interactions of bacterially-infected and surrounding uninfected cells in a monolayer [6]. The model reproduces the mechanical gradient in the cell monolayer at a particular stage of infection when some cells are infected, but collective extrusion of infected cells is not yet observed (8-16 h. post-infection). Additionally, we have also inferred how cellular mechanical variables such as cell-cell junctional forces, cell-ECM adhesion forces or the cell protrusion law regulate the outcome of infected cell squeezing and cell protrusion. According to our initial objectives, we have delineated: (1) the importance of cell-ECM adhesions in ruling the mechanical competition of cells in infected monolayers; (2) the relevance of cell-cell junctions in force transduction between cells and its influence on the formation of infection mounds; (3) the new quantitative protrusion law, which improves the performance of the model since the level of protrusion is proportional to the stress gradient that the given cell senses and not to on-off values fixed by the user.

Despite the new findings, our model still presents some limitations that are discussed below and can be the focus of future work. First, we are only simulating one single mechanotransduction cycle of contraction and protrusion in the cell, whereas in *in vitro* experiments, cells are constantly moving and deforming. In spite of this limitation, the protrusion of uninfected surrounding cells is sufficient in enabling us to observe *in silico* the initial squeezing of infected cells that drives the formation of the infection mound. In addition, the linear protrusion law (which is a simplification of the complex mechanical interactions of cells in the monolayer) improves the performance of the model as compared to the previous on-off law. The degree of infected cell squeezing in the new proposed model is more consistent with our previous

experimental observations in terms of cell-ECM adhesions, cellular traction stresses and presence or absence of cell-cell junctions [6]. With the implementation of the new model, the level of protrusion, and consequently, the degree of infected cell squeezing depends on the cell's mechanical stress asymmetry, and not on the biased user-dependent choice of the level of protrusion. Second, we consider a fixed number of infected cells for each simulation. This is a simplification since the number of infected cells changes over time due to *L.m.* replicating and disseminating intercellularly over the course of the infection. Thus in our current model we do not consider bacterial intercellular dissemination or replication. Future directions should be focused on incorporating into the model the ability of the bacteria to spread and replicate within the host cells and on understanding the mechanical alterations this produces. Third, new cell-cell junctions cannot be formed since the geometry of the junction is fixed, *i.e.*, since we do not model dynamic cell-cell interactions. This is a current limitation of our model, since we can only interfere directly in the mechanical parameters (material properties) assigned to the cell-cell junction. Future works could implement the formation of new cell-cell junctions by modelling cell-cell forces as external cues or by combining continuum models with agent-based models [50].

Various studies on cancer cells [51] as well as bacterially-exposed host cells [52, 53], have shown that alterations in human cell gene transcription can lead to production of matrix degrading enzymes, which can alter the composition and mechanical properties of the underlying ECM. That can lead to changes in the organization of the cytoskeleton and in the mechanical properties of the cells [51]. The polyacrylamide hydrogels that we manufacture are inert materials and thus cannot be degraded, therefore their stiffness cannot be altered. However, to enable cell attachment, polyacrylamide hydrogels are coated at their surface with collagen I. Therefore, host cells in principle could either degrade or deposit proteins onto it. This in turn could modulate adhesion of cells onto their matrix and in turn lead to alterations in the host cell cytoskeleton. However, at present we do not have data supporting this and RNA sequencing analysis of infected cells did not reveal upregulation of matrix metalloproteinases (typical matrix degrading enzymes) [6]. Future studies could determine whether infected cells have the ability to alter the composition of their ECM which in turn could modulate the organization of the cell cytoskeleton and biomechanics. If that turns out to be true, in the future we could account for changes in ECM mechanical properties in our model. Irrespective of the above, alterations in the cytoskeletal organization

of infected and surrounding uninfected cells as compared to cells never exposed to infection have been previously characterized and quantified in *in vitro* experiments [6]. The same applies to changes in the traction forces and monolayer stresses of both cell populations as compared to cells never exposed to infection [29].

As a future step, it is essential to incorporate the dynamic response of the cells into the model, as there are important changes in the configuration and the mechanical properties of the cell monolayer that are not accounted for in the current model. For example, *in vitro* experiments clearly demonstrate that the collective movement of infected cells is very different from that of cells never exposed to bacteria [29]. The monolayer of cells not exposed to infection is solid-like, since cells move very slowly, randomly and subdiffusively under confluence when they are caged by their neighbours. However upon infection, a transition takes place and cells start moving much faster and with a certain directionality (towards the center of the infection focus). The cells are in a superdiffusive state during infection and the whole monolayer behaves more like a fluid. This phase transition is a result of alterations in the interaction forces between cells [6]. This solid-to-fluid phase transition has also been observed in bronchial epithelial cell monolayers when exposed to compressive forces such as those that occur during bronchospasm in asthmatic patients [54]. Such phase transitions are thought to be related to changes in cell-cell and cell-ECM adhesions which can result in response to extracelullar physical cues but also in response to infection [6]. A previous study simulated this phase transition [55] in endothelial monolayers that migrate during wound closure, by a combination of continuous and discrete models (agent-based models and finite element methods). However, phase transitions that can occur in the context of infection have not yet been studied through numerical modelling. This can be the focus of future *in silico* studies.

Understanding also how bacterial infections modify the mechanical properties of cells is important to unravel how bacteria manage to disseminate, and how physical cues crosstalk with biochemical signals. The alteration of host cell mechanics by intracellular bacteria has recently been the focus of investigations thanks to new technological developments (*e.g.* traction force microscopy, atomic force microscopy, FRET sensors) [8]. Yet how the cellular monolayers as a whole, that is, the reaction of both infected and surrounding uninfected cells, change is still not fully uncovered. New tools and approaches to address the problem at the multicellular scale will help

answer these questions.

Different types of bacteria can alter in different ways the physical forces produced by their host cells to promote their own dissemination through tissues. In turn, the biochemical and physical environment surrounding host cells and bacteria can also distinctly impact those interactions [8]. In this work, we have developed our computational model to simulate intracellular infection with *L.m.* as a common intracellular bacterial pathogen model. Most of the input parameters of our model are based on measurements conducted during *in vitro* infection of host cells with *L.m.* However, our *in silico* model could be modified to study infection processes triggered by other intracellular bacterial pathogens. Based on previous experimental observations of *L.m.*-infected monolayers [6], in our simulations neighbouring uninfected cells protrude towards the infection focus centre. However, in different types of cellular competition there might be different types of cell motion observed. For example, in the context of cell overpopulation or during oncogenic transformation of cells, it is possible that the two competing cell groups might move in different ways compared to the ones considered herein [56]. In that case our model could be modified following a different protrusion law.

In the context of bacterial infection, mound formation has been observed *in vitro* in cell monolayers that were infected with *L.m.* and a mutant of *Rickettsia parkeri* (*R.p.*) [6]. The pathogenicity mechanisms of intracellular bacteria are sophisticated and diverse, and even bacteria that employ actin-based motility to spread from one host cell to another (like *Rickettsia parkeri*, or *Shigella flexneri*) do so employing distinct strategies some of which are still to be discovered [8]. We recently showed that the changes in host cell force transduction that *L.m.*-infected host cells undergo are modulated by innate immune signaling, and particularly NF-$\boldsymbol{\kappa B}$ activation, and thus intracellular bacteria that suppress host cell NF-$\boldsymbol{\kappa B}$ activation like *Rickettsia parkeri* do not elicit formation of infection mounds at late times post-infection [6]. However, following infection with a mutant of *R. parkeri* that lacks the outer surface protein B (OspB) and therefore cannot suppress NF-$\boldsymbol{\kappa B}$ activation, we did observe mounds. Whether additional intracellular pathogens that also activate NF-$\boldsymbol{\kappa B}$, including viruses, would induce infected cell extrusion using mechanisms similar to those observed during infection with *L.m.*, has not yet been explored but it is highly possible and remains to be uncovered [57, 58]. To that end, one would have to perform infection assays with different intracellular bacterial pathogens and characterize the changes in the biomechanics that emerge during the course of infection (*e.g.*, cell stiffness,

cell shape, cell motility traction forces, monolayer stresses) and accordingly modify the parameter inputs of the computational model.

By introducing other new modifications, the model could reproduce new scenarios such as more complex geometries by considering substrate curvature [59] or a geometry that is more similar to the *in vivo* condition (formation of crypts and villi structures). *In vivo*, not only the 3D topology of the intestinal epithelium is different but also the many other extracellular physical forces which cells are exposed to, and which are crucial in modulating cellular functions and intestinal barrier integrity [8]. In recently published work, using the on-off model we examined how the stiffness of the extracellular matrix where cells reside impacts the competition that arises between infected and uninfected cells [29]. The model predicted more infected cell extrusion on stiffer as opposed to softer substrates which we then confirmed experimentally. The model was also able to predict that increased traction stresses of surrounding uninfected cells on stiffer as opposed to softer matrices drive the enhanced collective extrusion of infected cells. Integrating into our model additional forces acting *in vivo* in the intestinal epithelium (*e.g.*, shear fluid flows, peristaltic strains) and examining *in silico* and *in vitro* how those impact infection processes is along our future goals. We believe that computational models will play a key role in linking *in vivo* and *in vitro* experiments, since one can get new insight from the results of the simulations and reach casual conclusions that can be then tested experimentally. Nevertheless, the 3D *in vivo* conditions in the intestinal monolayer are more complex than the conditions in 2D *in vitro* monolayers [60], but the application of 3D intestinal organoids *in vitro* can serve as a more tractable intermediate step [61]. Unlike *in vivo* bacterial infections, where so many variables change concurrently, using organoids or organ-on-chip devices one can emulate infection in a much more controllable system. Such systems can also more easily allow us to measure different biomechanical properties and are thus preferred for feeding in the future our computational model.

From the results of this computational work, we have learned:

1. When placed in close proximity to an infection domain, neighbouring uninfected cells need to exert higher traction stresses on their ECM to migrate towards and to squeeze infected cells. This process is essential for the collective extrusion of infected cells that follows. The lack of those strong cell-ECM adhesions makes cells unable to generate the displacements of infected cells and consequently the formation of the

mound.

2. Cell-cell junctions are required for the communication and force transduction between cells. To act collectively and force the squeezing of infected cells, neighbouring uninfected cells close to the infection focus require cell-cell contacts and the ability to transduce forces through them. In the absence of these cell-cell junctions, cells are not able to sense their mechanical environment and to elicit the collective extrusion of infected cells out of the monolayer.
3. The new protrusion law that we propose takes into account the stress gradient that neighbouring cells sense, being more unbiased (user - dependent) and consistent with previous cell mechanosensing mechanisms [37] than the simple on-off law we used previously.

Overall, our *in silico* model elucidates how changes in mechanical parameters of cells or their environment impact infected cell squeezing which is necessary for the collective infected cell extrusion we observe *in vitro*. We find that the protrusion and the behavior of surrounding uninfected cells as well as the modulation of cell-cell and cell-ECM adhesions crucially modulate this competition that arises during infection. However, there are still open questions related to how cell mechanics and signaling in concert impact such cell competitions and how the physical microenvironment can further modulate those. A better understanding of these processes will help future studies to discover new therapeutic strategies to fight infection.

7. Declaration of Competing Interest

The authors declare that they have no known competing financial interests or personal relationships that could have appeared to influence the work reported in this paper.

8. Acknowledgements

We are grateful to Libera Lo Presti for revising the manuscript. We also thank Julie A. Theriot for her insight and scientific discussions.

9. Funding

This work was supported by Grant PID2021-124271OB-I00 founded by MCIN/AEI/10.13039/501100011033 (R.A-Y and M.J.G-B) and ERDF A

way of making Europe (R.A-Y and M.J.G-B), the European Research council (ICoMICS Adv grant agreement: 101018587, (R.A-Y, J.M.G-A and M.J.G-B)), the Spanish Ministry of Universities (grant FPU 20/05274 (R.A-Y)) and Deutsche Forschungsgemeinschaft (DFG, German Research Foundation) under Germany's Excellence Strategy – EXC 2124 – 390838134 (E.E.B., M.M.).

References

[1] L. Radoshevich, P. Cossart, Listeria monocytogenes: towards a complete picture of its physiology and pathogenesis, Nature Reviews Microbiology 16 (2017) 32–46. doi:10.1038/nrmicro.2017.126.

[2] E. F. S. Authority, E. C. for Disease Prevention, C. (EFSA, ECDC), Ecdc the european union summary report on trends and sources of zoonoses, zoonotic agents and food-borne outbreaks in 2017, EFSA Journal (2018). doi:10.2903/j.efsa.2018.5500.

[3] E. Tambo, C. Yah, M. G, Deadly listeriosis outbreaks in south africa and australia: Re-inforcing food safety surveillance and emergency response actions, Journal of Advances in Virology Research 1 (2018) 1–7.

[4] M. Pentecost, G. Otto, J. Theriot, M. R. Amieva, Listeria monocytogenes invades the epithelial junctions at sites of cell extrusion, PLOS Pathogens 2 (2006) 1–12. doi:10.1371/journal.ppat.0020003.

[5] M. A. Grant, B. Wacław, R. J. Allen, P. Cicuta, The role of mechanical forces in the planar-to-bulk transition in growing *Escherichia coli* microcolonies, Journal of The Royal Society Interface 11 (2014) 20140400. doi:10.1098/rsif.2014.0400.

[6] E. E. Bastounis, F. Serrano-Alcalde, P. Radhakrishnan, P. Engstrom, M. J. Gómez-Benito, M. S. Oswald, Y.-T. Yeh, J. G. Smith, M. D. Welch, J. M. García-Aznar, J. A. Theriot, Mechanical competition triggered by innate immune signaling drives the collective extrusion of bacterially infected epithelial cells, Developmental Cell 56 (2021) 443–460. doi:10.1016/j.devcel.2021.01.012.

[7] R. Aparicio-Yuste, M. Muenkel, K. Axarlis, M. J. Gómez-Benito, A. Reuss, G. Blacker, M. Caspi Tal, P. Kraiczy, E. E. Bastounis, Borrelia burgdorferi modulates the physical forces and immunity signaling in endothelial cells, iScience (2022) 104793. doi:10.1016/j.isci.2022.104793.

[8] E. E. Bastounis, P. Radhakrishnan, C. K. Prinz, J. A. Theriot, Mechanical forces govern interactions of host cells with intracellular bacterial pathogens, Microbiology and Molecular Biology Reviews (2022) e0009420. doi:10.1128/mmbr.00094-20.

[9] R. L. Lamason, E. Bastounis, N. M. Kafai, R. Serrano, J. C. del Álamo, J. A. Theriot, M. D. Welch, Rickettsia sca4 reduces vinculin-mediated intercellular tension to promote spread, Cell 167 (2016) 670–683.e10. doi:10.1016/j.cell.2016.09.023.

[10] D. E. Ingber, Cellular mechanotransduction: putting all the pieces together again, The FASEB Journal 20 (2006) 811–827. doi:10.1096/fj.05-5424rev.

[11] T. Rajabian, B. Gavicherla, M. Heisig, S. Müller-Altrock, W. Goebel, S. D. Gray-Owen, K. Ireton, The bacterial virulence factor InlC perturbs apical cell junctions and promotes cell-to-cell spread of listeria, Nature Cell Biology 11 (2009) 1212–1218. URL: https://doi.org/10.1038/ncb1964. doi:10.1038/ncb1964.

[12] C. Faralla, E. E. Bastounis, F. E. Ortega, S. H. Light, G. Rizzuto, L. Gao, D. K. Marciano, S. Nocadello, W. F. Anderson, J. R. Robbins, J. A. Theriot, A. I. Bakardjiev, Listeria monocytogenes inlp interacts with afadin and facilitates basement membrane crossing, PLOS Pathogens 14 (2018) e1007094. doi:10.1371/journal.ppat.1007094.

[13] E. E. Bastounis, P. Radhakrishnan, C. K. Prinz, J. A. Theriot, Volume measurement and biophysical characterization of mounds in epithelial monolayers after intracellular bacterial infection, STAR Protocols 2 (2021) 100551. doi:10.1016/j.xpro.2021.100551.

[14] R. Löhner, H. Antil, J. M. Gimenez, S. Idelsohn, E. Oñate, A deterministic pathogen transmission model based on high-fidelity physics, Computer Methods in Applied Mechanics and Engineering (2022) 114929. doi:10.1016/j.cma.2022.114929.

[15] M. Kim, J. Park, M. Kang, J. Yang, W. Park, Gain and loss of antibiotic resistant genes in multidrug resistant bacteria: One health perspective, Journal of Microbiology 59 (2021) 535–545. doi:10.1007/s12275-021-1085-9.

[16] K. Bisht, R. Marathe, Rectification of twitching bacteria through narrow channels: A numerical simulations study, Physical Review E 101 (2020). doi:10.1103/physreve.101.042409.

[17] R. Jasevičius, R. Baronas, H. Kruggel-Emden, Numerical modelling of the normal adhesive elastic–plastic interaction of a bacterium, Advanced Powder Technology 26 (2015) 742–752. doi:10.1016/j.apt.2015.04.010.

[18] J. J. Winkle, O. A. Igoshin, M. R. Bennett, K. Josic, W. Ott, Modeling mechanical interactions in growing populations of rod-shaped bacteria, Physical Biology 14 (2017) 055001. doi:10.1088/1478-3975/aa7bae.

[19] F. Ivančić, T. W. Sheu, M. Solovchuk, The free surface effect on a chemotaxis–diffusion–convection coupling system, Computer Methods in Applied Mechanics and Engineering 356 (2019) 387–406. doi:10.1016/j.cma.2019.07.030.

[20] M. Doumic, S. Hecht, D. Peurichard, A purely mechanical model with asymmetric features for early morphogenesis of rod-shaped bacteria micro-colony, Mathematical Biosciences and Engineering 17 (2020) 6873. doi:10.3934/mbe.2020356.

[21] M. Delarue, J. Hartung, C. Schreck, P. Gniewek, L. Hu, S. Herminghaus, O. Hallatschek, Self-driven jamming in growing microbial populations, Nature Physics 12 (2016) 762–766. doi:10.1038/nphys3741.

[22] F. E. Ortega, E. F. Koslover, J. A. Theriot, Listeria monocytogenes cell-to-cell spread in epithelia is heterogeneous and dominated by rare pioneer bacteria, eLife 8 (2019). doi:10.7554/elife.40032.

[23] G. Limbert, R. Bryan, R. Cotton, P. Young, L. Hall-Stoodley, S. Kathju, P. Stoodley, On the mechanics of bacterial biofilms on non-dissolvable surgical sutures: A laser scanning confocal microscopy-based finite element study, Acta Biomaterialia 9 (2013) 6641–6652. doi:10.1016/j.actbio.2013.01.017.

[24] D. Feng, I. Neuweiler, U. Nackenhorst, Numerical simulation of 2d multi-species bacterial biofilm growth using the combined tdg-fic finite element method, in: VI International Conference on Computational Bioengineering, ICCB 2015, 2015, pp. 371–385.

[25] A. Velic, T. Tesfamichael, Z. Li, P. K. Yarlagadda, Parametric study on nanopattern bactericidal activity, Procedia Manufacturing 30 (2019) 514–521. doi:10.1016/j.promfg.2019.02.072.

[26] N. Kandemir, W. Vollmer, N. S. Jakubovics, J. Chen, Mechanical interactions between bacteria and hydrogels, Scientific Reports 8 (2018). doi:10.1038/s41598-018-29269-x.

[27] D. Volfson, S. Cookson, J. Hasty, L. S. Tsimring, Biomechanical ordering of dense cell population, Proceedings of the National Academy of Sciences 105 (2008) 15346–15351. doi:10.1073/pnas.0706805105.

[28] E. E. Bastounis, Y.-T. Yeh, J. A. Theriot, Subendothelial stiffness alters endothelial cell traction force generation while exerting a minimal effect on the transcriptome, Scientific Reports 9 (2019). doi:10.1038/s41598-019-54336-2.

[29] R. Aparicio-Yuste, M. Muenkel, A. Clark, M. J. Gomez-Benito, E. E. Bastounis, A stiff extracellular matrix favors the mechanical cell competition that leads to extrusion of bacterially-infected epithelial cells, Frontiers Cell Developmental Biology 10 (2022). doi:10.3389/fcell.2022.912318.

[30] S. A. Gudipaty, J. Rosenblatt, Epithelial cell extrusion: Pathways and pathologies, Seminars in Cell & Developmental Biology 67 (2017) 132–140. doi:10.1016/j.semcdb.2016.05.010.

[31] A. Villars, R. Levayer, Collective effects in epithelial cell death and cell extrusion, Current Opinion in Genetics & Development 72 (2022) 8–14. doi:10.1016/j.gde.2021.09.004.

[32] J. Y. Co, M. Margalef-Catalá, X. Li, A. T. Mah, C. J. Kuo, D. M. Monack, M. R. Amieva, Controlling epithelial polarity: A human enteroid model for host-pathogen interactions, Cell Reports 26 (2019) 2509–2520.e4. doi:10.1016/j.celrep.2019.01.108.

[33] L. A. Knodler, B. A. Vallance, J. Celli, S. Winfree, B. Hansen, M. Montero, O. Steele-Mortimer, Dissemination of invasiveSalmonellavia bacterial-induced extrusion of mucosal epithelia, Proceedings of the National Academy of Sciences 107 (2010) 17733–17738. doi:10.1073/pnas.1006098107.

[34] C. Schwayer, M. Sikora, J. Slováková, R. Kardos, C.-P. Heisenberg, Actin rings of power, Dev. Cell 37 (2016) 493–506. doi:10.1016/j.devcel.2016.05.024.

[35] J. Escribano, R. Sunyer, M. T. Sánchez, X. Trepat, P. Roca-Cusachs, J. M. García-Aznar, A hybrid computational model for collective cell durotaxis, Biomechanics and Modeling in Mechanobiology 17 (2018) 1037–1052. doi:10.1007/s10237-018-1010-2.

[36] R. Sunyer, V. Conte, J. Escribano, A. Elosegui-Artola, A. Labernadie, L. Valon, D. Navajas, J. M. García-Aznar, J. J. Muñoz, P. Roca-Cusachs, et al., Collective cell durotaxis emerges from long-range intercellular force transmission, Science 353 (2016) 1157–1161.

[37] B. Ladoux, R.-M. Mège, X. Trepat, Front–rear polarization by mechanical cues: From single cells to tissues, Trends in Cell Biology 26 (2016) 420–433. doi:10.1016/j.tcb.2016.02.002.

[38] D.-H. Kim, D. Wirtz, Cytoskeletal tension induces the polarized architecture of the nucleus, Biomaterials 48 (2015) 161–172. doi:https://doi.org/10.1016/j.biomaterials.2015.01.023.

[39] E. Bastounis, R. Meili, B. Álvarez González, J. Francois, J. C. del Álamo, R. A. Firtel, J. C. Lasheras, Both contractile axial and lateral traction force dynamics drive amoeboid cell motility, The Journal of cell biology 204 (2014) 1045–1061. doi:10.1083/jcb.201307106.

[40] E. Bastounis, B. n. Álvarez González, J. C. del Álamo, J. C. Lasheras, R. A. Firtel, Cooperative cell motility during tandem locomotion of amoeboid cells, Molecular Biology of the Cell 27 (2016) 1262–1271. doi:10.1091/mbc.E15-12-0836.

[41] C. Borau, R. Kamm, J. García-Aznar, Mechano-sensing and cell migration: a 3d model approach, Physical Biology 8 (2011) 066008. doi:10.1088/1478-3975/8/6/066008.

[42] P. Moreo, J. M. García-Aznar, M. Doblaré, Modeling mechanosensing and its effect on the migration and proliferation of adherent cells, Acta Biomaterialia 4 (2008) 613–621. doi:10.1016/j.actbio.2007.10.014.

[43] A. Nieto, J. Escribano, F. Spill, J. M. García-Aznar, M. J. Gómez-Benito, Finite element simulation of the structural integrity of endothelial cell monolayers: A step for tumor cell extravasation, Engineering Fracture Mechanics 224 (2020). doi:10.1016/j.engfracmech.2019.106718.

[44] S. Hervás-Raluy, J. M. García-Aznar, M. J. Gómez-Benito, Modelling actin polymerization: the effect on confined cell migration, Biomechanics and Modeling in Mechanobiology 18 (2019) 1177–1187. doi:10.1007/s10237-019-01136-2.

[45] L. Vujosevic, V. Lubarda, Finite-strain thermoelasticity based on multiplicative decomposition of deformation gradient, Theoretical and Applied Mechanics (2002) 379–399. doi:10.2298/tam0229379v.

[46] J.-F. Ganghoffer, 3 - constitutive models of soft and hard living tissues, in: J.-F. Ganghoffer (Ed.), Multiscale Biomechanics, Elsevier, 2018, pp. 149–186. doi:10.1016/B978-1-78548-208-3.50003-4.

[47] J. C. del Álamo, R. Meili, B. Álvarez González, B. Alonso-Latorre, E. Bastounis, R. Firtel, J. C. Lasheras, Three-dimensional quantification of cellular traction forces and mechanosensing of thin substrata by fourier traction force microscopy, PLOS ONE 8 (2013) 1–14. URL: https://doi.org/10.1371/journal.pone.0069850. doi:10.1371/journal.pone.0069850.

[48] J. Escribano, M. B. Chen, E. Moeendarbary, X. Cao, V. Shenoy, J. M. Garcia-Aznar, R. D. Kamm, F. Spill, Balance of mechanical forces drives endothelial gap formation and may facilitate cancer and immune-cell extravasation, PLOS Computational Biology 15 (2019) e1006395. doi:10.1371/journal.pcbi.1006395.

[49] M. Smith, ABAQUS/Standard User's Manual, Version 2020, Dassault Systèmes Simulia Corp, United States, 2020.

[50] I. González-Valverde, J. M. García-Aznar, Mechanical modeling of collective cell migration: An agent-based and continuum material approach, Computer Methods in Applied Mechanics and Engineering 337 (2018) 246–262. doi:10.1016/j.cma.2018.03.036.

[51] R. Kaukonen, A. Mai, M. Georgiadou, M. Saari, N. De Franceschi, T. Betz, H. Sihto, S. Ventelä, L. Elo, E. Jokitalo, J. Westermarck, P.-L. Kellokumpu-Lehtinen, H. Joensuu, R. Grénman, J. Ivaska, Normal stroma suppresses cancer cell proliferation via mechanosensitive regulation of jmjd1a-mediated transcription, Nature Communications 7 (2016) 12237. doi:10.1038/ncomms12237.

[52] J. Gebbia, J. Coleman, J. Benach, Borrelia spirochetes upregulate release and activation of matrix metalloproteinase gelatinase b (mmp-9) and collagenase 1 (mmp-1) in human cells, Infection and immunity 69 (2001) 456–62. doi:10.1128/IAI.69.1.456-462.2001.

[53] A. Behera, E. Hildebrand, J. Scagliotti, A. Steere, L. Hu, Induction of host matrix metalloproteinases by borrelia burgdorferi differs in human and murine lyme arthritis, Infection and immunity 73 (2005) 126–34. doi:10.1128/IAI.73.1.126-134.2005.

[54] J.-A. Park, L. Atia, J. A. Mitchel, J. J. Fredberg, J. P. Butler, Collective migration and cell jamming in asthma, cancer and development, Journal of Cell Science (2016). doi:10.1242/jcs.187922.

[55] I. González-Valverde, J. M. García-Aznar, An agent-based and FE approach to simulate cell jamming and collective motion in epithelial layers, Computational Particle Mechanics 6 (2018) 85–96. doi:10.1007/s40571-018-0199-2.

[56] A. Matamoro-Vidal, R. Levayer, Multiple influences of mechanical forces on cell competition, Current Biology 29 (2019) R762–R774. doi:10.1016/j.cub.2019.06.030.

[57] F. Abaitua, F. R. Zia, M. Hollinshead, P. O'Hare, Polarized cell migration during cell-to-cell transmission of herpes simplex virus in human skin keratinocytes, Journal of Virology 87 (2013) 7921–7932. doi:10.1128/JVI.01172-13.

[58] C. Beerli, A. Yakimovich, S. Kilcher, G. V. Reynoso, G. Fläschner, D. J. Müller, H. D. Hickman, J. Mercer, Vaccinia virus hijacks egfr signalling to enhance virus spread through rapid and directed infected cell motility, Nature Microbiology 4 (2019) 216–225. doi:10.1038/s41564-018-0288-2.

[59] M. Luciano, S.-L. Xue, W. De Vos, L. Redondo-Morata, M. Surin, F. Lafont, E. Hannezo, S. Gabriele, Cell monolayers sense curvature by exploiting active mechanics and nuclear mechanoadaptation, Nature Physics 17 (2021). doi:10.1038/s41567-021-01374-1.

[60] C. Pérez-González, G. Ceada, M. Matejčić, X. Trepat, Digesting the mechanobiology of the intestinal epithelium, Current Opinion in Genetics & Development 72 (2022) 82–90. doi:10.1016/j.gde.2021.10.005.

[61] M. Nikolaev, O. Mitrofanova, N. Broguiere, S. Geraldo, D. Dutta, Y. Tabata, B. Elci, N. Brandenberg, I. Kolotuev, N. Gjorevski, H. Clevers, M. Lutolf, Homeostatic mini-intestines through scaffold-guided organoid morphogenesis, Nature 585 (2020) 1–5. doi:10.1038/s41586-020-2724-8.

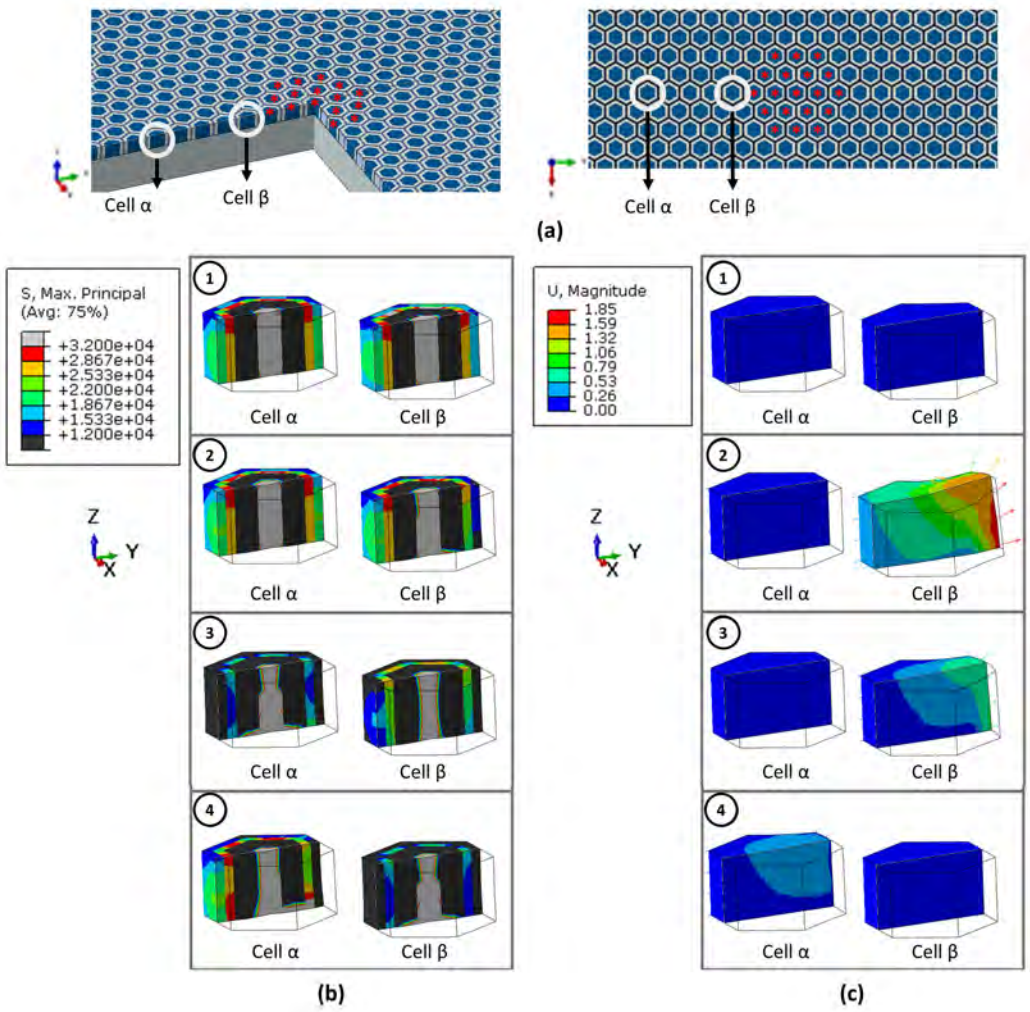

Figure 5: Maximum cellular principal stresses (Pa) and displacements (μm) in the cells when including the quantitative protrusion law proposed in equation 1. (a) Whole model in which the position of the two uninfected surrounding cells analysed is indicated (distal α and proximal β), red asterisks denote the infected cells. (b) Maximum principal stress (Pa) distribution in the passive part of cells α (distal) and β (proximal) during the contraction phase. (c) Displacements of α (distal) and β (proximal) cells during the protrusion phase. Different cases analysed: (1) uninfected cells cannot form new cell-ECM adhesions, (2) uninfected surrounding cells or β (proximal) cells can form new cell-ECM adhesions, (3) only uninfected cells close to the infection are able to create cell-cell junctions, (4) only uninfected cells far from the infection are able to create cell-cell junctions.

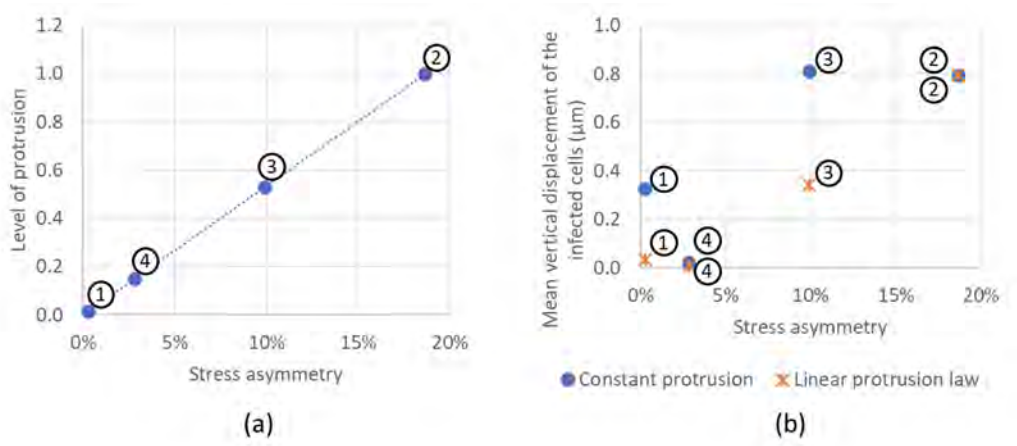

Figure 6: Protrusion degree and infected cell squeezing: (a) Plot showing the level of cellular protrusion (y-axis) versus degree of maximum stress asymmetry in the cell (x-axis) for the four cases considered; (b) Plot of the mean infected cell height (μm, y-axis) versus percentage of stress asymmetry (x-axis) considering the on-off protrusion law (blue points) and the asymmetry dependent protrusion-law (orange crosses) for the four cases analyzed. Different cases analysed: (1) none of the uninfected cells can form new cell-ECM adhesions; (2) only proximal uninfected surrounding cells can form new cell-ECM adhesions and all cells form cell-cell junctions; (3) only proximal uninfected surrounding cells are able to form cell-cell junctions but not distal ones; (4) only distal uninfected surrounding cells are able to create cell-cell junctions, but not proximal ones.

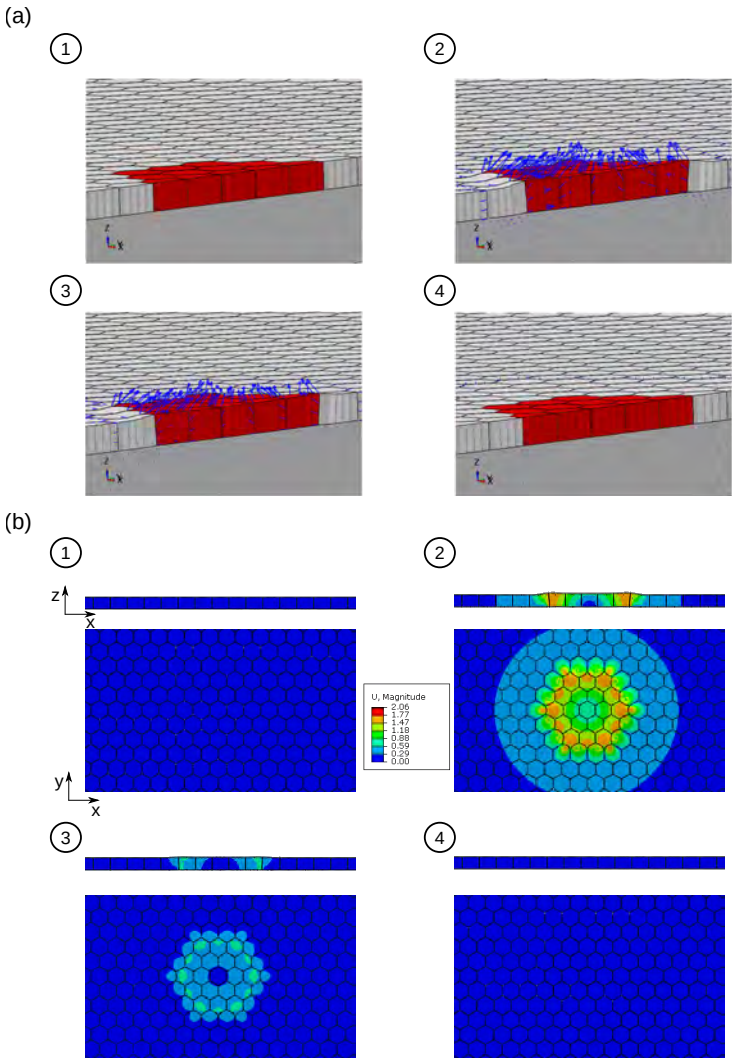

Figure 7: Simulation of cell competition results in infected cell squeezing. (a) Cross-sectional view of the cell monolayer and of the ECM on which cells reside. Blue arrows indicate cellular displacements during the protrusion phase which lead to infected cell squeezing. Infected cells are in red and uninfected cells in gray. Different cases analysed (1) uninfected cells cannot create new cell-ECM adhesions, (2) uninfected surrounding cells can create new cell-ECM adhesions, (3) only uninfected cells close to the infection focus are able to create cell-cell junctions, (4) only uninfected cells far from the infection focus are able to produce cell-cell junctions. (b) Cell monolayer displacements after one cycle of contraction and protrusion. Orthogonal view maps of the magnitude of cellular displacements. Top (x-y) and side (x-z) maps are shown in all the cases.